JOURNAL OF PROPULSION AND POWER
Vol. 24, No. 3, May–June 2008

Optimal Design of Hybrid Rocket Motors for Microgravity Platform

Lorenzo Casalino* and Dario Pastrone*
Politecnico di Torino, 10129 Torino, Italy

DOI: 10.2514/1.30548

A nested direct/indirect method is used to find the optimal design for a microgravity platform which is based on a hybrid sounding rocket. The direct optimization of the parameters that affect the motor design is coupled with the indirect trajectory optimization to maximize a given mission performance index. A gas-pressure feed system is used, with three different propellant combinations. The feed system exploits a pressurizing gas, namely, helium, when hydrogen peroxide or liquid oxygen is used as an oxidizer. The simplest blowdown design is compared with a more complex pressurizing system, which has an additional gas tank that allows for a phase with constant propellant tank pressure. Only self-pressurization is considered with nitrous oxide; two different models are used to describe the behavior of the tank pressurization. The simplest model assumes liquid/vapor equilibrium. A two-phase model is also proposed: Saturated vapor and superheated liquid are considered and the liquid/vapor mass transfer evaluation is based on the liquid spinodal line. Results show that the different tank-pressurization models yield minimal differences of the optimal motor characteristics. Performance differs slightly due to the different mass of the residual oxidizer. The propellant comparison for the present case shows better performance for hydrogen peroxide/polyethylene with respect to liquid oxygen/hydroxyl-terminated polybutadiene, while nitrous oxide/hydroxyl-terminated polybutadiene remains attractive for system simplicity and low costs.

Nomenclature

A_b	=	burning surface area, m^2
A_p	=	port area, m^2
A_t	=	nozzle throat area, m^2
a	=	regression constant, $m^{1+2n}\ kg^{-n}\ s^{n-1}$
C_F	=	thrust coefficient
c_l	=	liquid oxidizer specific heat capacity, $J/(kg \cdot K)$
c^*	=	characteristic velocity, m/s
$\boldsymbol{D}$	=	drag vector, N
D	=	rocket outer diameter, m
$\boldsymbol{F}$	=	thrust vector, N
F	=	thrust magnitude, N
G_O	=	oxidizer mass flux, $kg/(s \cdot m^2)$
$\boldsymbol{g}$	=	gravity acceleration, $m/(s^2)$
h	=	specific enthalpy, J/kg
h_{ev}	=	specific latent heat of vaporization, J/kg
J	=	throat area to initial port area ratio
L	=	overall length, m
L_b	=	fuel grain length, m
M	=	rocket mass, kg
m	=	mass, kg
m_{Ot}	=	mass of oxidizer in the tank, kg
n	=	mass-flux exponent
n_x	=	longitudinal acceleration, g
p	=	pressure, Pa
p_{din}	=	dynamic pressure, kPa
R	=	port radius, m
R_t	=	throat radius, m
$\boldsymbol{r}$	=	position vector, m
T	=	temperature, K
t	=	time, s
$t_{\mu g}$	=	time spent above 100 km, s
u	=	specific internal energy, J/kg
V	=	volume, m^3
$\boldsymbol{v}$	=	velocity vector, m/s
Z	=	hydraulic resistance, $1/(kg \cdot m)$
z	=	normalized altitude
α	=	mixture ratio
γ	=	specific heat ratio
ε	=	nozzle area ratio
Θ	=	vapor compressibility factor
ν	=	regression rate, m/s
ρ	=	density, kg/m^3

Subscripts

a	=	auxiliary gas
BD	=	beginning of blowdown phase
c	=	combustion chamber at nozzle entrance
cv	=	condensing vapor
e	=	nozzle exit
el	=	evaporating liquid
F	=	fuel
g	=	pressurizing gas
i	=	initial value
l	=	liquid oxidizer
lim	=	superheated liquid limit
O	=	oxidizer
p	=	overall propellant (oxidizer + fuel)
res	=	tank residual
sat	=	saturation
SL	=	sea level
sp	=	liquid spinodal line
t	=	oxidizer propellant tank
v	=	vapor oxidizer
0	=	ambient
1	=	combustion chamber at head end

Superscript

$\dot{}$	=	time derivative

Received 19 February 2007; revision received 30 October 2007; accepted for publication 17 December 2007.

*Associate Professor, Dipartimento di Energetica, Corso Duca degli Abruzzi, 24 Torino. Senior Member AIAA.

I. Introduction

HYBRID rocket motors (HRMs) present higher density impulse, when compared to liquid bipropellant rocket engines, and higher specific impulse, when compared to solid rocket motors and liquid monopropellant rockets. Moreover, they are safe and reliable, can be throttled within a wide thrust range, and have shutdown–restart capability. Last but not least, they are relatively low cost and have a reduced environmental impact. All these features make HRMs suitable for relatively simple low-cost applications, such as sounding rockets to be used as microgravity platforms. A large number of papers concerning numerical and experimental HRM investigation can be found in the literature [1–6]. In most numerical investigations, a parametric optimization is performed to find the best grain and nozzle geometries as well as the best operating conditions, such as mean mixture ratio and chamber pressure. The optimization of the motor design and operations is, however, strictly related to the type of mission considered. This is especially true in the present case, which considers a sounding rocket that performs a suborbital flight. Thrust has a major influence, because it affects both the motor design and the trajectory performance; a compromise must be sought, as greater thrusts reduce the gravitational losses while increasing drag losses and structural mass. Therefore, the design optimization should include trajectory analysis and, possibly, its optimization. The development of a code that couples motor design and trajectory optimization is the purpose of this paper.

The choice of the propellant combination has a major influence on a rocket design. Three propellant combinations are widely used today: hydrogen peroxide (HP)/polyethylene (PE), liquid oxygen (LOX)/hydroxyl-terminated polybutadiene (HTPB), and nitrous oxide (N2O)/HTPB. Nitrous oxide can be used either as a cryogenic liquid propellant or as a storable liquefied gas propellant at ambient temperature. In the latter case, N2O shows modest performance due to its low density and high vapor pressure, thus requiring heavy tanks. On the other hand, nitrous oxide presents some inherent attractive advantages, such as being nontoxic, stable, and comparatively unreactive at ordinary temperatures. In contrast with hydrogen peroxide, nitrous oxide does not require catalytic decomposition. Moreover, the aforementioned high vapor pressure at ambient temperature determines its self-pressurizing capability. This fact and the safety characteristics of N2O explain the wide use of nitrous oxide as an oxidizer in HRMs (as an example, a N2O/HTPB hybrid rocket was used for a manned suborbital flight to a 100-km altitude [7]). Nitrous oxide has also been tested with paraffin fuels [8], which yield superior regression rates, thus permitting the simplest single-port grain geometries, while preserving safety and nontoxicity [9] (liquefying hybrid).

The propellant tank-pressurization modeling plays a key role in predicting rocket performance. When a self-pressurizing propellant such as N2O is used, the mass flux between the two phases becomes a fundamental control mechanism of the tank pressure change. Unfortunately, existing theories seem to be unable to quantitatively predict this mass flux. Moreover, the tank-pressurization model has to be embedded into more complex design procedures and be accessed many times, thus relative simplicity is mandatory.

The simplest model that can be adopted assumes a saturated liquid–vapor mixture inside the tank: The propellant mass is treated as a homogeneous fluid and evaluation of liquid/vapor heat and mass transfer is not required. This model works well with low propellant mass flow rates, but this is not the case for sounding rockets, where more sophisticated models seem to be required. In a recent paper, Zilliac and Karabeyoglou [10] proposed to describe N2O tank self-pressurization with a lumped model, which considers three regions (bulk liquid, surface layer, and bulk vapor). The mass flux was calculated by applying the energy equation in steady-state conditions, written for the surface layer (which is supposed to be at the saturation temperature). This theory underpredicts the mass flux from liquid to vapor; thus an empirical factor had to be introduced to correct the heat transfer coefficient.

In this paper, a hybrid rocket motor is considered for powering a sounding rocket, which performs a suborbital flight via ground launch. The relevant motor design parameters are identified and their influence on performance investigated for the above mentioned propellant combinations. A gas-pressure feed system is assumed for HP/PE and LOX/HTPB combinations. To assess the benefit provided by the oxidizer mass flow control while facing complexity, the blowdown feed system option is first considered and then compared to a partially regulated pressure system. On the other hand, for the self-pressurized N2O/HTPB combination, the authors adopt two simple tank-pressurization models that do not require any evaluation of the liquid/vapor heat transfer rate: The classical aforementioned homogeneous model and a two-phase model that considers superheated liquid and saturated vapor. To analyze the model effect on performance and design parameters, these models are embedded into a hybrid direct/indirect optimization procedure, which couples the optimization of motor characteristics with trajectory optimization.

II. Ballistic Model

The performance of the three propellant combinations is evaluated [11] as a function of the mixture ratio α, assuming $p_c = 10$ bar. Even though the actual pressure in the combustion chamber can span over a wide range during motor operations, the error is small for chamber pressures and mixture ratios considered in this paper. Frozen equilibrium expansion is considered; the exhaust gas maintains throughout the nozzle the composition that it has in the combustion chamber. This conservative assumption of frozen equilibrium expansion is adopted to account for the low combustion efficiency of HRMs; in addition, a 0.96 c^*-efficiency [12] is introduced. Third-degree polynomial curves fitting the characteristic velocity and specific heat ratio are embedded in the code to compute the proper values as the mixture ratio changes during motor operations.

The regression rate is determined by the oxidizer mass flux

$$v = aG_O^n \tag{1}$$

The values of a and n are shown in Table 1, expressing G_O in $\mathrm{kg/(m^2\,s)}$ and v in m/s.

A single-port circular-section grain geometry is assumed, while considering a uniform regression rate along the port axis. The port radius differential equation (a dot indicates the time derivative) is

$$\dot{R} = v = a\left(\frac{\dot{m}_O}{A_p}\right)^n \propto \dot{m}_O^n R^{-2n} \tag{2}$$

No pyrolysis of the lateral ends is considered. Pressure losses inside the combustion chamber are taken into account by relating the chamber head-end pressure p_1 to the chamber nozzle-stagnation pressure p_c. An approximate relation, similar to that proposed by Barrere et al. [17] for side-burning grains, is used

$$p_1 = \left[1 + 0.2\left(\frac{A_t}{A_p}\right)^2\right] p_c \tag{3}$$

The hydraulic resistance Z in the oxidizer flow path from the tank to the combustion chamber determines the oxidizer flow rate. Under the assumption of incompressible turbulent flow

$$\dot{m}_O = \sqrt{(p_t - p_1)/Z} \tag{4}$$

The value of Z is assumed to be constant during motor operation. When N2O is used and the liquid phase ends, gaseous propellant flows from the propellant tank into the combustion chamber. In this

Table 1 Values of a and n to be used when v is m/s and G_O is $\mathrm{kg/(m^2\,s)}$ in Eq. (1)

Propellants	a	n	Source
HP/PE	7.00×10^{-6}	0.800	[13,14]
LOX/HTPB	9.24×10^{-6}	0.852	[15]
N2O/HTPB	1.87×10^{-4}	0.347	[16]

case the oxidizer mass flow through the injectors is evaluated assuming a choked flow. The value of the injection area is evaluated as a function of the hydraulic resistance. Assuming suitable values of injector discharge coefficient and liquid density, one obtains

$$\dot{m}_O = 1.59410^{-2}\sqrt{\frac{p_t m_{\mathrm{Ot}}}{ZV_t}} \tag{5}$$

where m_t is the gaseous N2O mass in the propellant tank. The fuel mass flow is

$$\dot{m}_F = \rho_F v A_b \propto \dot{m}_O^n R^{1-2n} \tag{6}$$

The mixture ratio is

$$\alpha = \frac{\dot{m}_O}{\dot{m}_F} \propto \dot{m}_O^{1-n} R^{2n-1} \tag{7}$$

An isentropic expansion in the nozzle is assumed, and the chamber nozzle-stagnation pressure p_c is determined by

$$p_c = \frac{(\dot{m}_O + \dot{m}_F)c^*}{A_t} \tag{8}$$

III. Motor Design

According to the chosen ballistic model, the design of the HRM is defined by 1) initial thrust level F_i, 2) initial mixture ratio α_i, 3) nozzle expansion ratio ε, 4) initial value of tank pressure $(p_t)_i$, 5) initial value of chamber pressure $(p_c)_i$, and 6) ratio J of the throat area to the initial port area.

The initial chamber pressure is assigned by imposing $(p_c)_i = 0.4(p_t)_i$; actually, the ratio p_t/p_c varies during operation, but the assumed initial ratio is usually sufficient to guarantee $p_t/p_c > 1.5$ and to avoid coupling between the hybrid motor and the oxidizer feed system. The initial port area to throat area ratio J should be as large as possible but not exceed 0.5 to avoid excessive pressure losses and nonuniform grain regression. Additional parameters are to be given, depending on the chosen oxidizer and feed system.

A. Gas-Pressure Feed System: Options and Parameters

Two different options are considered for a pressurizing feed system which uses compressed gas. Option 1 is a simple blowdown (BD) pressurization system. Option 2 consists of a phase with constant tank pressure, maintained by means of helium flowing from an auxiliary tank, followed by a blowdown phase. When option 1 is chosen, the gas is assumed to expand isentropically. The value of the initial ullage volume $(V_g)_i$ (or, equivalently, the mass of the pressurizing gas) is the only additional parameter. On the other hand, when option 2 is adopted, the initial ullage volume is assumed to be 3% of the tank volume, in order to have a stable regulator response when the outflow starts [18]. In this case two additional parameters are the auxiliary gas tank volume V_a and the initial pressurizing gas pressure p_a; the latter has a weak influence on the performance; thus $p_a = 200$ bar is assumed throughout. The parameter V_a is conveniently replaced by the exhausted oxidizer mass at the beginning of the blowdown phase $(m_O)_{\mathrm{BD}}$. When the tank pressure is kept constant $p_t = (p_t)_i$, whereas p_t is again calculated assuming an isentropic expansion of the pressurizing gas in the tank during the subsequent blowdown phase. Calling $(V_g)_{\mathrm{BD}}$ the gas volume in the propellant tank at the beginning of the blowdown phase

$$p_t = (p_t)_i\left[\frac{(V_g)_{\mathrm{BD}}}{V_g}\right]^\gamma \tag{9}$$

where $V_g = (V_g)_i + m_O/\rho_O$. Obviously $(V_g)_{\mathrm{BD}} = (V_g)_i$ when the simpler blowdown pressurization is chosen (option 1), otherwise $(V_g)_{\mathrm{BD}} = (V_g)_i + (m_O)_{\mathrm{BD}}/\rho_O$ for option 2. The design parameters are optimized as shown in Sec. V.

B. Self-Pressurizing Oxidizer: Parameters and Tank Pressure Models

For a self-pressurizing oxidizer, liquid and vapor are in equilibrium before motor operation and the tank pressure is only related to the temperature. An initial value of 45 bar (which corresponds to a temperature of 287.2 K) is assumed for $(p_t)_i$. Self-pressurization occurs until the liquid phase ends; an isentropic blowdown phase follows, ruled by

$$p_t = (p_t)_{\mathrm{BD}}\left[\frac{m_{\mathrm{Ot}}}{(m_{\mathrm{Ot}})_{\mathrm{BD}}}\right]^\gamma \tag{10}$$

To avoid poor combustion, the thruster is turned off when the pressure in the combustion chamber reaches 1 bar. The tank volume is determined by the indirect procedure during the trajectory optimization to obtain the prescribed pressure at burnout; a tentative starting value must be given to begin the procedure. The initial ullage volume is assumed to be 3% of the oxidizer tank volume. The remaining design parameters, namely, F_i, α_i, and ε, are optimized as shown later.

A model is needed to evaluate tank pressure during oxidizer outflow. Two simple models are here proposed; they both neglect heat transfer between the tank walls and the oxidizer. The homogeneous model assumes that both liquid and vapor are saturated at the same temperature. The two-phase model considers a saturated vapor and a warmer liquid phase; a pressure/temperature relation lying between the saturation line and the liquid spinodal line is prescribed for the liquid phase. These models are detailed in the following, including a comparison of the numerical results with experimental data presented by Van Pelt et al. [8].

1. *Homogeneous Model*

The simplest model [19] assumes the liquid and vapor phases at uniform temperature, that is, equal to the saturation temperature of N2O at the tank pressure. No additional pressurizing gas is considered, and the oxidizer mass (liquid plus vapor inside the tank, subscript t) is assumed to be in a homogeneous state. Its thermodynamic properties are mass averaged. A control surface corresponding to the inside surface of the tank wall is defined and the first law of thermodynamics and the law of conservation of mass are applied to the resulting control volume. The oxidizer leaves the tank as saturated liquid, with specific enthalpy $h_{l,\mathrm{sat}}$, and the tank pressure derivative is expressed by

$$\dot{p}_t = -\frac{\dot{m}_O[h_{l,\mathrm{sat}} - h_t - \rho_t(\partial h_t/\partial \rho_t)_p]}{\rho_t V_t(\partial u_t/\partial p_t)_\rho} \tag{11}$$

This solution represents an upper limit of the propellant tank pressure, because it implies that a well-mixed liquid (without stratification) exchanges energy with vapor at an infinite rate.

2. *Two-Phase Lumped Model*

Liquid and vapor are not in equilibrium during motor operation when a fast expansion occurs: A temperature gradient exists inside the tank, with the liquid being warmer than the vapor. A two-region (bulk liquid and bulk vapor) simplified lumped model is here adopted, with wall heat transfer being neglected. Liquid and vapor are considered to be in equilibrium before motor operation. During operation their temperatures are assumed to be uniform (i.e., no stratification effects are taken into account) albeit distinct. Condensation ($\dot{m}_{\mathrm{cv}}$) and evaporation/boiling ($\dot{m}_{\mathrm{el}}$) are taken into account at the vapor–liquid interface.

The general form of energy conservation for a variable control volume enclosing an unsteady open process is applied, with both kinetic and potential energy being neglected. It is assumed that the condensing vapor leaves the ullage volume as saturated liquid with $T = T_v$, and that the evaporating liquid enters the ullage volume with saturated vapor enthalpy at $T = T_l$. One obtains, for a control volume enclosing the vapor phase (i.e., the ullage volume)

$$m_v \frac{\mathrm{d}u_v}{\mathrm{d}T_v}\dot{T}_v - \dot{m}_{\mathrm{cv}}\left[h_{\mathrm{ev}}(T_v) - \frac{p_t}{\rho_v}\right] - \dot{m}_{\mathrm{el}}[h_v(T_l) - u_v] = -p_t\dot{V}_v \tag{12}$$

where u_v is the saturated vapor specific internal energy at T_v, $h_v(T)$ is the saturated vapor specific enthalpy, and $h_{\mathrm{ev}}(T)$ is the specific latent heat of vaporization. The rate of vapor volume change

$$\dot{V}_v = \frac{\dot{m}_l}{\rho_l} - \frac{m_l}{\rho_l^2}\left(\frac{\partial\rho_l}{\partial T_l}\dot{T}_l + \frac{\partial\rho_l}{\partial p_t}\dot{p}_t\right) \approx \frac{\dot{m}_l}{\rho_l} - \frac{m_l}{\rho_l^2}\frac{\mathrm{d}\rho_{l\mathrm{sat}}}{\mathrm{d}T_l}\dot{T}_l \tag{13}$$

is computed by approximating the density of the liquid with its value at saturation conditions. For the liquid phase, the temperature rate of the bulk liquid is approximated by the relation

$$c_l m_l \dot{T}_l = \dot{m}_{\mathrm{cv}}[h_l(T_v) - h_l(T_l)] - \dot{m}_{\mathrm{el}}h_{\mathrm{ev}}(T_l) \tag{14}$$

where $h_l(T)$ is the specific enthalpy of the saturated liquid. Mass conservation is expressed by

$$\dot{m}_l = \dot{m}_{\mathrm{cv}} - \dot{m}_{\mathrm{el}} - \dot{m}_O; \qquad \dot{m}_v = \dot{m}_{\mathrm{el}} - \dot{m}_{\mathrm{cv}} \tag{15}$$

Finally the real gas equation of state requires

$$\frac{\dot{p}_t}{p_t} + \frac{\dot{V}_v}{V_v} = \frac{\dot{m}_v}{m_v} + \frac{\mathrm{d}\Theta}{\mathrm{d}T_v}\frac{\dot{T}_v}{\Theta} + \frac{\dot{T}_v}{T_v} \tag{16}$$

where the vapor compressibility factor Θ is evaluated on the saturation line.

It is assumed that condensation occurs ($\dot{m}_{\mathrm{cv}} \neq 0$) and that the vapor phase follows the saturation line. One has

$$\dot{p}_t = \frac{\mathrm{d}p_{\mathrm{sat}}}{\mathrm{d}T_v}\dot{T}_v \tag{17}$$

No liquid evaporation/boiling is considered ($\dot{m}_{\mathrm{el}} = 0$) until the liquid reaches a limiting pressure p_{lim}, which lies between the saturation line and the spinodal line. After reaching p_{lim}, evaporation/boiling takes place and the liquid is constrained to satisfy a given relation, namely, $p_t = p_{\mathrm{lim}}(T_l)$. Therefore

$$\dot{p}_t = \frac{\mathrm{d}p_{\mathrm{lim}}}{\mathrm{d}T_l}\dot{T}_l \tag{18}$$

Equation (18) allows for the evaluation of $\dot{m}_{\mathrm{el}}$; thus, not needing a liquid/vapor heat transfer rate evaluation, the model complexity is greatly reduced.

3. *Numerical Results Comparison*

In an interesting paper [8], experimental data of N2O tank-pressurization history during motor operation are presented. They permit a meaningful comparison with the tank-pressurization models used in the present paper. As the true oxidizer mass flow was not measured in [8], a mean mass flow rate had to be assumed to carry out the calculations. The comparison is shown in Fig. 1.

The relation between the tank pressure and the temperature of the liquid during evaporation/boiling in the two-phase model is given by

$$p_{\mathrm{lim}}(T_l) = \frac{p_{\mathrm{sat}}(T_l) + p_{\mathrm{sp}}(T_l)}{2} \tag{19}$$

A model [20] for the limit of homogeneous bubble nucleation is used to evaluate the pressure p_{sp} along the liquid spinodal line as a function of the temperature of the liquid. The following fitting linear relation is assumed:

$$p_{\mathrm{sp}} = 1.98T_l - 540 \tag{20}$$

where T_l is expressed in K and p_{sp} in bar. Figure 1 shows that, as expected, the homogeneous model overpredicts the tank pressure while, with the exception of the ignition transient, the two-phase model, although underpredicting the tank pressure, yields a better approximation of the experimental data. Even though better accuracy

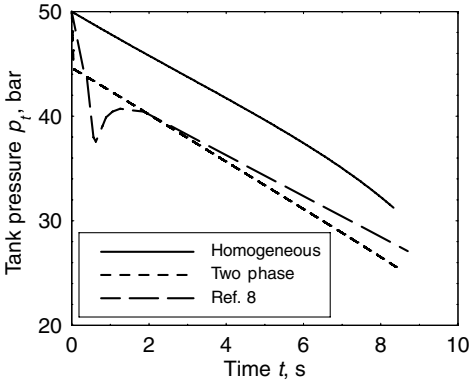

Fig. 1 Comparison of N2O calculated tank pressure with experimental data from [8].

can of course be obtained by conveniently modifying Eq. (19), this example shows how simple hypotheses can allow a reasonable estimation of the pressure history.

IV. Initial Motor Geometry and Motor Operation

Given the set of design parameters, the motor geometry is determined. The relevant properties of the combustion gases can be first computed, owing to the fact that the initial values of c^* and γ can be calculated from α_i via the aforementioned curve fittings. The thrust coefficient C_F can then be evaluated by assuming an isentropic one-dimensional expansion with constant γ, provided the ambient pressure is known. With a 0.98 correction factor introduced to modify the vacuum thrust coefficient, one obtains

$$C_F = 0.98\left\{\sqrt{\frac{2\gamma^2}{\gamma-1}\left(\frac{2}{\gamma+1}\right)^{\frac{\gamma+1}{\gamma-1}}\left[1 - \left(\frac{p_e}{p_c}\right)^{\frac{\gamma}{\gamma-1}}\right]} + \varepsilon\frac{p_e}{p_c}\right\} - \varepsilon\frac{p_0}{p_c} \tag{21}$$

The mass flow rates at rocket ignition (i.e., at $t = 0$) are found from the initial thrust F_i

$$(\dot{m}_p)_i = (1+\alpha_i)(\dot{m}_F)_i = \frac{1+\alpha_i}{\alpha_i}(\dot{m}_O)_i = \frac{F_i}{c_i^*(C_F)_i} \tag{22}$$

The throat and initial port areas A_t and $(A_p)_i$ are then determined

$$A_t = \frac{(\dot{m}_p)_i}{(p_c)_i c_i^*}; \qquad (A_p)_i = \frac{A_t}{J} \tag{23}$$

The nozzle throat area A_t is considered to be constant during operation. One also finds

$$(A_b)_i = \frac{(A_p)_i^n}{a\rho_F}\frac{(\dot{m}_F)_i}{(\dot{m}_O)_i^n} \tag{24}$$

The initial port radius R_i and the fuel grain length L_b are then obtained, thus defining the initial motor geometry. The head-end pressure is computed with Eq. (3) and, knowing the initial tank pressure, also the hydraulic resistance Z can be determined by applying Eq. (4) at $t = 0$. The motor geometry is completely defined and, once V_t has been assumed, the motor performance can be evaluated during operation.

The tank pressure rules motor operation. When LOX or HP are used as an oxidizer, either $p_t = (p_t)_i$ or p_t is provided by Eq. (9). On the other hand, with N2O as the oxidizer, Eq. (11) must also be integrated when the homogeneous model is chosen. When the two-phase model is adopted and some liquid phase is present in the tank, the tank pressure history can be obtained by integrating the differential system consisting of Eqs. (12–17), and, when required, Eq. (18), concerning tank pressure, liquid, and vapor temperature and mass transfer rates. Equation (10) is instead used for both models when the liquid phase ends.

Numerical integration of Eqs. (2), (4), and (6), allows the evaluation of the fuel grain geometry and oxidizer and fuel masses and mass flows. Equation (5) replaces Eq. (4) during the N2O blowdown phase. At each instant t, once the tank pressure p_t and the motor geometry are known, the propellant flow rates (and their ratio α), c^* and p_c are computed by numerically solving Eqs. (2–8), while the curve fit for c^* as a function of α is used. Then, the thrust level $F = p_c A_t C_F$ is determined by evaluating C_F at the actual altitude via Eq. (21), to integrate the trajectory equations. At burnout the overall propellant and structural mass are easily evaluated. For the self-pressurizing case, the residual gaseous mass in the oxidizer tank is also obtained.

V. Optimization

The optimization procedure aims at finding the motor design parameters and the corresponding trajectory that maximize the mission performance index, which is, in this paper, the time spent above a 100-km altitude. As the number of motor design parameters is low (five when using HP or LOX, three when using N2O), their optimization is easily carried out by a direct method. Also, the relations, which determine the motor behavior, cannot be written explicitly and indirect methods cannot be used. On the other hand, the trajectory optimization may be characterized by continuous controls (namely, the thrust direction), which would either require a discretization by means of a large number of parameters or the use of indirect methods. A mixed optimization procedure [21] is here adopted. An indirect method [22] optimizes the trajectory for each choice of the motor parameters. These are instead optimized by means of a direct procedure [23]. Both methods have been developed at the Politecnico di Torino.

Tentative values are initially assumed for the design parameters. F_i, α_i, and ε are the optimization parameters when N2O is the self-pressurizing oxidizer; F_i, α_i, ε, $(p_t)_i$ and either $(V_g)_i$ (option 1) or $(m_O)_{\mathrm{BD}}$ (option 2) are the set of optimization variables when a gas-pressure feed system is considered. For each set of parameters the fast and accurate indirect procedure, in a few seconds, provides the optimal trajectory and the corresponding performance index when a 2 GHz PC is used. The design parameters are then varied by small quantities to numerically evaluate the derivatives of the performance index with respect to the design parameters. To find the performance index maximum, a procedure based on Newton's method is then used to determine the set of design parameters which simultaneously nullify the index partial derivatives. Only a few minutes are sufficient to obtain the optimal design and the corresponding trajectory.

A point mass rocket is considered for the trajectory optimization. The state equations [21] provide the derivatives of position $\boldsymbol{r}$ (radius, latitude, and longitude), velocity $\boldsymbol{v}$ (radial, eastward, and northward components) and rocket mass M. In a vectorial form one has

$$\frac{\mathrm{d}\boldsymbol{r}}{\mathrm{d}t} = \boldsymbol{v} \qquad \frac{\mathrm{d}\boldsymbol{v}}{\mathrm{d}t} = \boldsymbol{g} + \frac{\boldsymbol{F} - \boldsymbol{D}}{m} \qquad \frac{\mathrm{d}M}{\mathrm{d}t} = -\frac{|\boldsymbol{F}|}{c} \tag{25}$$

An inverse-square gravity field is assumed. Exponential fits are used to describe the atmosphere density and pressure

$$\frac{\rho_0}{\rho_{\mathrm{SL}}} = \exp(-1938.0 z^{1.150}) \qquad \frac{p_0}{p_{\mathrm{SL}}} = \exp(-1839.6 z^{1.118}) \tag{26}$$

where z is the vehicle altitude normalized with the Earth's radius.

The equations of motion are written in nondimensional form to improve the integration's numerical accuracy. The trajectory is split into phases with homogeneous control law. In the present case, the trajectory consists of the following: a ramp ascent, zero-lift gravity-turn thrust phase, coast to reach 100 km, coast above 100 km. A 6 m ramp is considered; the inclination relative to the vertical direction is subject to optimization. The propelled phase assumes the thrust to be parallel to the relative velocity, due to the fact that sounding rockets do not usually feature complex guidance systems. In this specific case, the direct optimization could also deal with the trajectory parameters, but the indirect formulation of the trajectory optimization problem is maintained so that more general control laws could also be considered.

The details of the indirect optimization procedure can be found in [21] and are here only summarized. An adjoint variable is associated with each equation; the theory of optimal control provides the Euler–Lagrange equations for the adjoint variables, algebraic equations that determine the control variables (in this case, no explicit control is present during the trajectory as thrusting is assumed to be along the rocket axis), and the boundary conditions for optimality. The multipoint boundary value problem, which arises from the application of the theory of optimal control, is solved by a procedure [24] based on Newton's method. Tentative values are initially chosen for the problem unknowns and progressively modified to fulfill the boundary conditions. The unknown parameters are the time lengths of each phase, that is, ramp ascent, constant tank pressure thrusting (option 2 only), self-pressurized thrusting (N2O/HTPB only), blowdown thrusting, coast to 100 km, and coast above 100 km. Additional unknowns are the ramp inclination, rocket diameter (which is chosen to have an L/D aspect ratio equal to 12), the radius adjoint variable after the start of the coast phase above 100 km, and finally the initial values of the adjoint variables associated with mass, radius, latitude, eastward and northward velocity components. The oxidizer tank volume is an additional parameter in the case of self-pressurizing oxidizer. It is determined to consume the whole of the liquid oxidizer at the end of the self-pressurized phase. The oxidizer mass in the tank at the start of the blowdown phase $(m_{\mathrm{Ot}})_{\mathrm{BD}}$ is an additional unknown when option 2 is adopted for the gas-pressure feed system.

No constraints (dynamic pressure, acceleration) are imposed during the trajectory optimization, because the results show that typical limits of present-technology sounding rockets are not exceeded. Constraints could be easily introduced into the optimization procedure, whenever required (e.g., by limiting the initial thrust).

VI. Numerical Results

The optimization procedure, which has been described in the previous section, is now applied to the trajectory of a sounding rocket with the aim of maximizing the time $t_{\mu g}$ spent above 100 km, which is conventionally considered to be in microgravity conditions. It has been verified that $t_{\mu g}$ differs by less that 5 s from the time during which the rocket actually experiences a state of free fall, with drag acceleration lower than 1 μg. For simplicity, the trajectory is assumed to lie on the equatorial plane, but the optimization procedure is capable of handling three-dimensional trajectories.

The rocket initial mass is 500 kg, with 100 kg reserved for payload and other masses, which are not related to propulsion system characteristics (e.g., avionics). The remaining 400-kg mass budget has to be shared between propellants, combustion chamber, nozzle, tanks, and rocket casing. The combustion chamber has a 6-mm insulating liner (with density equal to that of the solid fuel) and an aluminum alloy cylindrical wall. The cylindrical propellant tank has a diameter which is determined by the optimization procedure, which seeks a compromise between drag loss reduction and minimal structural mass. The wall thickness of the propellant tank is determined assuming a 1.25 safety factor. The rocket diameter is a consequence of the propellant tank diameter; a 1-mm aluminum case is assumed. A rocket length (except the payload) to outer diameter ratio of 12 is imposed. A 45-deg convergent and a 20-deg divergent nozzle with a phenolic silica ablative layer are considered. A uniform thickness is assumed and is evaluated according to [25], using average values of the transport properties and heat flux. The nozzle mass is computed accordingly; the structural mass is small compared to the ablative layer mass and is thus neglected.

Because an accurate estimation of the drag coefficient is not a simple task for a small rocket, a sensitivity study has been conducted to analyze the drag effects. Results show that drag affects performance, but the optimal design does not present relevant changes. Results are presented in the following, using a simplified

Table 2 Optimal design and performance for different propellant combinations and feed systems

Propellants	N2O model/feed option	F_i, kN	α_i	ε	$(p_t)_i$, bar	m_p, kg	m_{res}, kg	$t_{\mu g}$, s	R_t, m	D, m	L, m
N2O/HTPB	Homogeneous	13.2	9.37	4.57	45.0	328	20.5	140	0.042	0.40	4.77
N2O/HTPB	Two phase	16.2	10.92	4.14	45.0	340	8.7	177	0.046	0.40	4.75
LOX/HTPB	Option 1	23.5	3.20	4.53	59.9	328	0.9	219	0.047	0.46	5.52
HP/PE	Option 1	20.5	7.19	5.83	65.6	339	0.9	299	0.048	0.42	5.01
HP/PE	Option 2	16.4	8.02	4.66	38.3	348	1.1	328	0.051	0.41	4.91

drag model: A 0.2 drag coefficient is assumed for all the considered cases, with a reference area equal to the rocket cross section.

The N2O/HTPB rocket characteristics and the corresponding trajectory are optimized for both the homogeneous and two-phase tank pressure models. The results are compared in Table 2 to the performance of hybrid rockets with different propellant combinations (namely, LOX/HTPB and HP/PE), which use either a blowdown pressurization (option 1) or present a constant-pressure phase (option 2), with helium as the pressurizing gas. The optimal trajectories are shown in Fig. 2.

The optimization procedure determines the initial values of thrust, mixture ratio, and nozzle expansion area ratio (the initial tank pressure and the pressurizing gas mass are also optimized for LOX/HTPB and HP/PE), which maximize the time spent above 100 km. The optimal values of the design parameters are dictated by the kind of influence they have on the trajectory performance. Large values of initial thrust do reduce the gravitational losses, but also increase drag losses and require a heavier motor. The mixture ratio must ensure a large specific impulse, but also influences the structural mass. The nozzle expansion area ratio is indeed related to the chamber pressure, because an expansion to ambient pressure is desirable. Both p_c and the ambient pressure are decreasing as the tank pressure diminishes and the rocket rises, but usually p_c decreases more slowly, and a compromise value must be sought. The flow is slightly overexpanded at liftoff, whereas it is underexpanded at high altitudes. A lower nozzle expansion ratio is required when the initial tank pressure is low.

The lower performance of the N2O/HTPB rocket is due to two factors: First, it is related to the lower specific impulse of this propellant combination compared to the HP/PE and LOX/HTPB combinations. The performance is further penalized by the large amount of gaseous N2O that remains in the tank (m_{res}) leaving it useless for propulsion, when compared to the lower helium mass of the other two cases. Because of the fact that final values of tank temperature and pressure are different, the computed N2O gaseous mass, which remains inside the tank, also depends on the tank-pressurization model and affects the performance. On the other hand, the optimal characteristics of the rocket are only slightly dependent on the model. Only the rapid pressure drop of the two-phase model at startup has to be taken into account with some adjustments. The N2O pressure and temperature histories inside the oxidizer tank are shown in Figs. 3 and 4. The thrust is presented in Fig. 5, which also shows, for the sake of comparison, the thrust histories for the LOX/HTPB and HP/PE propellant combinations. It is worth noting that self-pressurization allows for a more uniform thrust profile, but this, in turn, produces large acceleration levels during the final part of the self-pressurized thrusting phase (Fig. 6). A higher peak dynamic pressure is therefore found when a comparison is made with the blowdown pressurization cases, as shown in Fig. 7. On the other

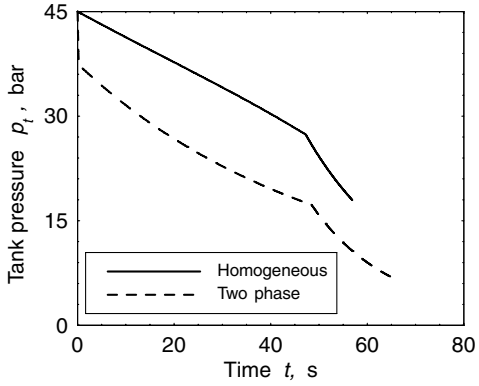

Fig. 3 Pressure history in the N2O oxidizer tank.

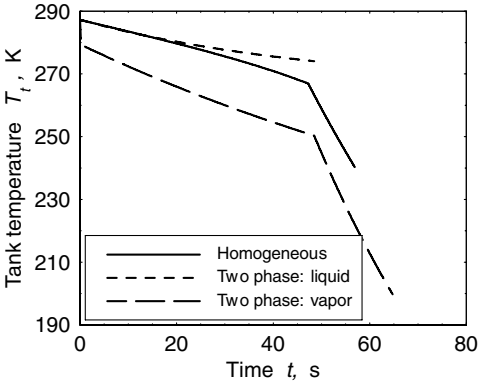

Fig. 4 Temperature history in the N2O oxidizer tank.

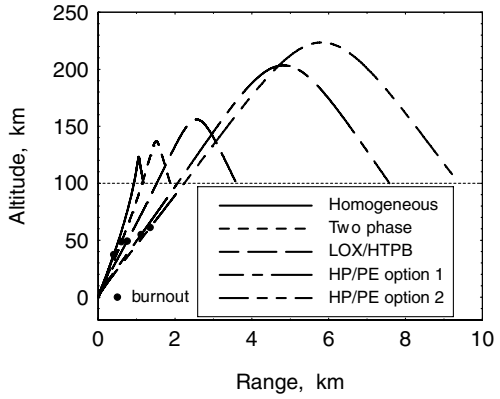

Fig. 2 Ascent trajectories for different propellant combinations and feed systems.

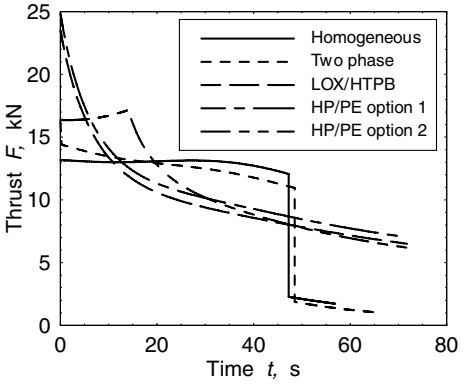

Fig. 5 Thrust history.

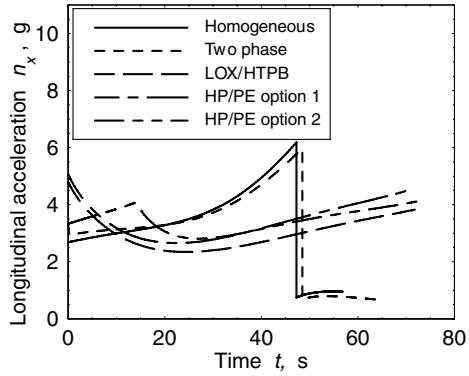

Fig. 6 Longitudinal acceleration history.

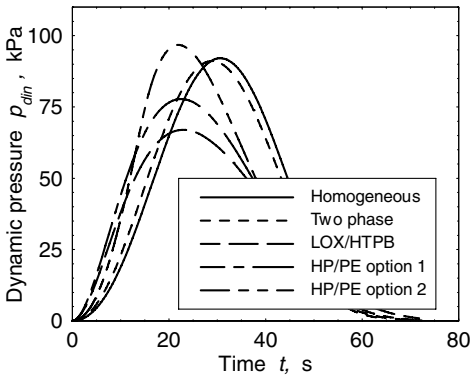

Fig. 7 Dynamic pressure history.

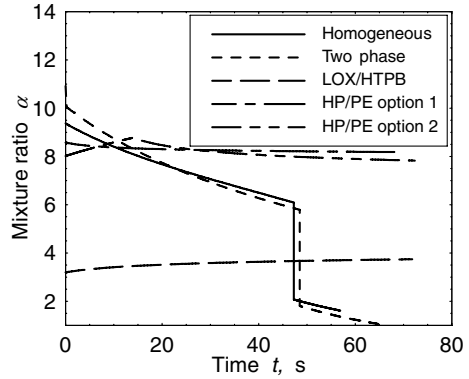

Fig. 8 Mixture-ratio history.

hand, the greater acceleration reduces the thrusting time. One should note the rapid decrease in pressure and temperature that occurs when the liquid phase vanishes, and the corresponding discontinuity both in thrust and acceleration due to the oxidizer's flow rate change.

The mixture-ratio shifting is larger for the self-pressurizing N2O/HTPB combination (see Fig. 8). The mixture ratio α is proportional to $m_O^{1-n}R^{2n-1}$. When $n > 0.5$ (HP/PE and LOX/HTPB), the increase in the port radius compensates for the decrease of the oxidizer flow rate, and only small variations occur. When $n < 0.5$ (N2O/HTPB) both terms decrease and the mixture ratio rapidly falls during operation. The mean value for α of the N2O/HTPB combination (6.94 for the homogeneous model and 6.73 for the two-phase model) is not very far from the value which maximizes the specific impulse, that is, $\alpha = 7$. The difference is related to the need to keep the structural mass low, without excessively penalizing the specific impulse.

Microgravity times obtained with LOX/HTPB are roughly 25% lower than those given by HP/PE. The lower performance is mainly due to the greater fuel mass (the mixture ratio which provides the maximum specific impulse is roughly 2 instead of 6.7), which, in turn, requires a longer grain and heavier combustion chamber and case. Even though a compromise value is adopted for the mixture ratio (the average α is 3.52), the structural mass is greater, thus less propellant mass is available, offsetting the benefits related to the larger specific impulse of the LOX/HTPB propellant combination. A different grain geometry may ease this problem.

When a phase with constant tank pressure is introduced, the optimization parameters remain, as before, the initial values of thrust, mixture ratio, pressure in the propellant tank, and the nozzle expansion area ratio; the pressurizing gas mass is not considered as a parameter, but is conveniently replaced by the exhausted oxidizer mass $(m_O)_{\mathrm{BD}}$ at the start of the blowdown phase, and is calculated a posteriori. The results obtained for the most promising propellant combination, namely, HP/PE, are presented, and the blowdown case (option 1) is compared with the partially regulated pressure case (option 2).

The introduction of an initial phase with constant tank pressure improves the performance; as in the previous cases, the advantage is related to the larger propellant mass (due to the reduction of the structural mass) rather than to the larger mean specific impulse. The regulated operation allows for a lower pressure inside the propellant tank, and the tank wall thickness (1.9 mm versus 3.1 mm for the blowdown case) and tank mass (13 kg versus 28 kg) are greatly reduced. The mass of the pressurizing gas tank is instead only about 6.6 kg.

Even though the initial thrust of the blowdown case is greater, it rapidly decreases because of the decreasing tank pressure, as shown in Fig. 9. The rocket acceleration diminishes (notwithstanding the mass reduction) and rapidly becomes lower than that of the partially regulated pressure case (option 2). The acceleration grows during the phase when p_t is held constant (see Fig. 6) because of the mass reduction and thrust increment due to the ambient pressure decrease, while the rocket is rising through the atmosphere. The rocket acceleration is therefore more vigorous and produces the greatest dynamic pressure.

Figure 8 shows the effect of the feed system design on the mixture ratio trend, which can either grow or decrease, depending on port radius and oxidizer flow rate, in agreement with Eq. (7). For HP/PE, α grows slightly during the constant-pressure phase of option 2, whereas it shows a small decrease during blowdown; α instead grows during the blowdown phase when the LOX/HTPB combination is adopted. For the HP/PE combination the average values for α are roughly 8.3 (option 1) and 8.2 (option 2), quite far from the value which provides the maximum specific impulse (about 6.7). As in the case of the LOX/HTPB combination, it is preferable to increase the oxidizer mass to reduce both grain length and structural mass.

When options 1 and 2 are compared, the peak acceleration is almost the same. The peak is at the final point for the blowdown case, whereas it is at the end of the constant tank pressure phase when option 2 is considered. The larger acceleration during the initial phase produces the largest maximum value of dynamic pressure.

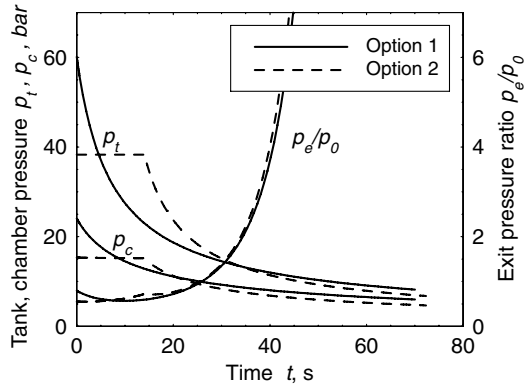

Fig. 9 Pressure history for HP/PE propellant combination using options 1 and 2.

VII. Conclusions

Direct and indirect optimization procedures, both developed at the Politecnico di Torino, have been suitably nested to couple the optimization of the parameters affecting the hybrid rocket design with the trajectory optimization. The optimization method appears to be fast and reliable and has been successfully applied to a microgravity platform. This platform consists of a ground-launched single-stage hybrid sounding rocket designed to perform a suborbital flight.

The analysis yields results which are similar to those obtained when the mixture-ratio control of liquid rocket engines is analyzed for ascent trajectories: The optimum solutions require mean mixture ratios that are larger than the value which maximizes the specific impulse, in order to reduce the structural mass. A propellant combination comparison shows the benefit of using propellants which have a high specific impulse for large mixture ratios such as HP/PE. Compared to combinations which have high specific impulse with low mixture ratios, such as LOX/HTPB, HP/PE permits a shorter grain and a lower structural mass, thus increasing the propellant fraction and the trajectory performance. The benefit of the partial regulation of the tank pressure has also been discussed; the improvement is mainly due to the structural mass reduction, as the presence of the regulated phase allows a lower pressure in the propellant tank, thus reducing its mass (on the other hand, structural loads are increased). Also the use of nitrous oxide as a self-pressurizing oxidizer has been investigated. Even though the performance, in terms of microgravity time, is lower compared to other propellant combinations, a N2O/HTPB hybrid rocket can provide access to space and offer a viable option for low-cost as well as high-safety sounding rockets.

Along with a more classical homogeneous model, a simple two-phase description of the N2O in tank behavior has been developed. This model does not require liquid/vapor heat transfer evaluation to deal with evaporation/boiling during motor operation. The results of the motor optimization depend only slightly on the chosen tank pressure model: The optimal grain geometry is only barely modified, the thrust profile has similar characteristics, and the difference in performance is only related to the gaseous oxidizer remaining in the tank, considered to be useless for thrust generation.

An experimental investigation of the performance prediction is required to assess the accuracy of the computed results, especially as far as the regression rates are concerned. They have a strong influence on the engine design and performance, and may also significantly alter the results.

References

[1] Dyer, J., Doran, E., Dunn, Z., Lohner, K., Bayart, C., Sadhwani, A., Zilliac, G., Cantwel, B., and Karabeyoglu, M. A., "Design and Development of a 100 km Nitrous Oxide/Paraffin Hybrid Rocket Vehicle," AIAA Paper 2007-5362, July 2007.

[2] Kwon, S. T., Park, B. K., Lee, C., and Lee, J., "Optimal Design of Hybrid Motor for the First Stage of Air Launch Vehicle," AIAA Paper 2003-4749, July 2003.

[3] Sackheim, R., Ryan, R., and Threet, E., "Survey of Advanced Booster Option for Potential Shuttle-Derivative Vehicles," AIAA Paper 2001-3414, July 2001.

[4] Schoonover, P. L., Crossley, W. A., and Heister, S. D., "Application of a Genetic Algorithm to the Optimization of Hybrid Rockets," *Journal of Spacecraft and Rockets*, Vol. 37, No. 5, 2000, pp. 622–629.

[5] Vonderwell, D. J., Murray, I. F., and Heister, S. D., "Optimization of Hybrid-Rocket-Booster Fuel-Grain Design," *Journal of Spacecraft and Rockets*, Vol. 32, No. 6, 1995, pp. 964–969.

[6] Jansen, D. P. F. L., and Kletzkine, P., "Preliminary Design for a 3 kN Hybrid Propellant Engine," *ESA Journal*, Vol. 12, No. 4, 1988, pp. 421–439.

[7] Dornheim, M. A., "Reaching 100 km," *Aviation Week and Space Technology*, Vol. 161, No. 6, Aug. 2004, pp. 45, 46.

[8] Van Pelt, D., Hopkins, J., Skinner, M., Buchanan, A., Gulman, R., Chan, H., Karabeyoglu, M. A., and Cantwell, B., "Overview of a 4-Inch OD Paraffin-Based Hybrid Sounding Rocket Program," AIAA Paper 2004-3822, July 2004.

[9] Karabeyoglu, M. A., Altman, D., and Cantwell, B. J., "Combustion of Liquefying Hybrid Propellants: Part 1, General Theory," *Journal of Propulsion and Power*, Vol. 18, No. 3, 2002, pp. 610–620.

[10] Zilliac, G., and Karabeyoglu, M. A., " Modeling of Propellant Tank Pressurization," AIAA Paper 2005-3549, July 2005.

[11] Mc Bride, B. J., Reno, M. A., and Gordon, S., "CET93 and CETPC: An Interim Updated Version of the NASA Lewis Computer Program for Calculating Complex Chemical Equilibria with Applications," NASA TM-4557, March 1994.

[12] Sutton, G. P., and Biblarz, O., *Rocket Propulsion Elements*, 7th ed., Wiley, New York, 2001, p. 64.

[13] Maisonneuve, Y., Godon, J. C., Lecourt, R., Lengelle, G., and Pillet, N., "Hybrid Propulsion for Small Satellites: Design Logic and Test," *Combustion of Energetic Materials*, Begell House, New York, 2002, pp. 90–100.

[14] Wernimont, E. H., and Heister, S. D., "Combustion Experiments in Hydrogen Peroxide/Polyethylene Hybrid with Catalitic Ignition," *Journal of Propulsion and Power*, Vol. 16, No. 2, 2000, pp. 318–326.

[15] Rocker, M., "Modeling of Nonacoustic Combustion Instability in Simulations of Hybrid Motor Tests," NASA TP-000-209905, Feb. 2000.

[16] Doran, E., Dyer, J., Lohner, K., Dunn, Z., Cantwell, B., and Zilliac, G., "Nitrous Oxide Hybrid Rocket Motor Fuel Regression Rate Characterization," AIAA Paper 2007-5352, July 2007.

[17] Barrere, M., Jaumotte, A., De Veubeke, B. F., and Vandenkerckhove, J., *Rocket Propulsion*, Elsevier, New York, 1960, pp. 251–256.

[18] Brown, C. D., *Spacecraft Propulsion*, AIAA Education Series, AIAA, Reston, VA, 1996, p. 82.

[19] Lin, C. S., Van Dresar, N. T., and Hasan, M. M., "Pressure Control Analysis of Cryogenic Storage Systems," *Journal of Propulsion and Power*, Vol. 20, No. 3, 2004, pp. 480–485.

[20] Delale, C. F., Hruby, J., and Marsik, F., "Homogeneous Bubble Nucleation in Liquids: The Classical Theory Revisited," *Journal of Chemical Physics*, Vol. 118, No. 2, 2003, pp. 792–806. doi:10.1063/1.1525797

[21] Casalino, L., and Pastrone, D., "Optimal Design and Control of Hybrid Rockets for Access to Space," AIAA Paper 2005-3547, July 2005.

[22] Casalino, L., Colasurdo, G., and Pastrone, D., "Optimal Low-Thrust Escape Trajectories Using Gravity Assist," *Journal of Guidance, Control, and Dynamics*, Vol. 22, No. 5, 1999, pp. 637–642.

[23] Casalino, L., and Pastrone, D., "Oxidizer Control and Optimal Design of Hybrid Rockets for Small Satellites," *Journal of Propulsion and Power*, Vol. 21, No. 2, 2005, pp. 230–238.

[24] Colasurdo, G., and Pastrone, D., "Indirect Optimization Method for Impulsive Transfer," AIAA Paper 94-3762, Aug. 1994.

[25] Barker, D. H., Kording, J. W., Belnap, R. D., and Hall, A. F., "A Simplified Method of Predicting Char Formation in Ablating Rocket Exit Cones," *AIChE Chemical Engineering Progress Symposium Series*, American Institute of Chemical Engineers, New York, 1965, Vol. 61, No. 59, pp. 108–114.

S. Son
Associate Editor